Thin smectic liquid crystalline fibrils of chiral rodlike particles

A. Kuhnhold* and V. Tänzel
Institute of Physics, University of Freiburg, 79104 Freiburg (Breisgau), Germany

(Received 9 March 2021; revised 26 July 2021; accepted 9 August 2021; published 31 August 2021)

Inspired by recent experimental work on virus-polymer mixtures, we study the properties of thin smectic fibrils composed of chiral rodlike particles using Monte Carlo simulations. Due to the interplay between surface energy, elastic deformation energy, and entropic effects, the fibril's layers relax into a twisted state. We focus our study on the layers' twist direction and map our results to the antiferromagnetic Ising model. In this view, the chiral interaction mimics an external field that drives the layers to have the same sense of twist. Besides, we determine the free energy difference and barrier height between an alternating and a nonalternating sequence of twisted layers composed of achiral rods and find that an alternating sequence is slightly preferred. We also see that the fibrils contract on increasing the chiral interaction strength and think that further studies on self-assembled functional materials can use our results.

DOI: 10.1103/PhysRevE.104.024703

I. INTRODUCTION

Systems of rodlike bacteriophages and viruses have found much attention as model liquid crystals in the recent decades [1–3]. The variety of self-assembled structures that arise in mixtures of such rodlike particles with depleting agents (usually added polymer in the globular phase) has been the focus of many studies [4–9]. Controlling the self-organization of the anisotropic particles is of great importance for functional materials, biomimetic applications, and nanotechnology. The effective attraction between the colloidal rods due to the presence of the depletants can easily be tuned by changing the depletant concentration and their effective size. Not only the depletants but also the properties of the colloidal particles determine the type and behavior of the self-assembled structures. Thus, the goal is to be able to control the constituent-structure-property relation.

For the paper at hand, we take one of the structures found in experiments and explore its behavior using Monte Carlo simulations. The chosen structure is called a smectic fibril and can be described as a thin fiber formed by elongated particles whose centers of mass arrange in layers. In another view, this is a stack of colloidal membranes, which are one-layer thick disklike (or hexagonally shaped) assemblies of the rodlike particles. An illustrative snapshot is shown in Fig. 1. The rods that constitute the fibril have a chiral pair interaction in addition to their hard core repulsion. Why chiral particles? The system's parameter space already includes the size and aspect ratio of the rods, size ratio of rods and depletants, number of rods, and concentration of depletants. Chirality adds another dimension to it that helps to tune the properties of materials. It is also known that viruses as constituents of self-assembled structures, which give our work inspiration, are chiral objects. Their chirality is different from one type of virus to another and can be modified by mutation [11,12].

The growth of smectic fibrils can follow different routes: (i) colloidal membranes grow first and then assemble to a stack and (ii) particles assemble to a columnar fibril first and then undergo a columnar-smectic transition. Experiments have shown that the mechanism depends on the strength of the attractive depletion interaction [9]. If the attraction is strong, then columnar fibrils are found; however, the columnar-smectic transition is rarely seen because of kinetic trapping. More often, route (i) is considered, for which theoretical descriptions and simulations are available [6,13,14]. In this paper, we take already grown fibrils and focus on the influence of the strength of a chiral interaction between the rodlike particles that form the fibril. This influence has already been discussed for colloidal membranes [7,15,16], but to our knowledge, not for stacks of those. The obvious difference is that the membrane faces are either exposed to the depletant gas (isolated membranes) or another membrane face (in fibrils). We expect to see a differing behavior because the shape and structure of individual membranes explicitly depend on their surface. The system finds its equilibrium state by minimizing its free energy, where the latter can be approximated by a sum of elastic deformation energy and surface energy terms. Thus, the different interfaces must lead to different membrane states.

Immediately visible from the snapshot in Fig. 1 is that the rods do not point along the fibril axis (at least those close to the surface) but show some twist. We will discuss the sense and the sequence of the twists and map left- and right-handed membranes to spin states up and down in a $1d$ Ising model description.

II. MODEL AND SIMULATIONS

As a model for rods that constitute the smectic fibrils, we use spherocylinders with a hard core. The spherocylinders' dimensions are the length L and the diameter D. In this study, the aspect ratio is kept constant at $L/D = 10$, and D is used as the length unit. Spheres of diameter D are added as a second

*anja.kuhnhold@physik.uni-freiburg.de

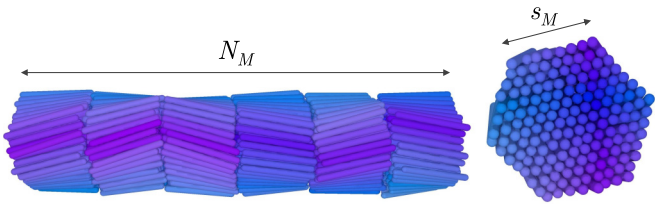

FIG. 1. Rendered snapshot of an equilibrated fibril with dimensions $s_M = 8$ (number of rods at the side of the hexagon) and $N_M = 6$ (number of stacked membranes). Left: side view; right: top view. Different senses of the twists' direction can be seen. The color codes the orientation of rods, and the rendering was done using POV-Ray [10]. Not shown are the depleting spheres that stabilize the structure.

component. They are so-called Asakura-Oosawa spheres, i.e., they do not interact with each other but have a hard core interaction with the rods that gives rise to a depletant force between them. For sufficiently strong resulting attraction, the assembled structures are stabilized. To avoid explicitly dealing with a large number of spheres, an implicit method introduced by Glaser *et al.* has been utilized, keeping the chemical potential of the depletants, μ_D, constant [17]. The essential point is that the spheres are not stored as permanent objects but are only temporarily created to check for overlaps with the rods; for details, we refer to the original publication [17].

To set up the fibrils' initial configuration, we first assemble rods on a hexagonal grid, standing upright parallel to each other. Together, they form a membrane in the shape of a regular hexagon. We have chosen this shape in order to mimic the structure found in experiments of *fd* virus-polymer (polyethylene glycol) mixtures [9]. The number of spherocylinders making up a hexagon side is denoted s_M. Next, N_M membranes are stacked along the x axis, building a fibril that spans the simulation box. An equilibrated configuration is depicted in Fig. 1.

In addition to the spherocylinders' hard core, a chiral pair potential that is known to form a cholesteric bulk phase is added [18,19]:

$$U_G(\vec{r}_{ij}, \hat{m}_i, \hat{m}_j) = -\varepsilon \frac{(\hat{m}_i \cdot \hat{m}_j)}{(r_{ij}/D)^7}[(\hat{m}_i \times \hat{m}_j) \cdot \hat{r}_{ij}], \qquad (1)$$

where $\hat{m}_i$, $\hat{m}_j$ denote the orientations of two rods and $\hat{r}_{ij} = \vec{r}_{ij}/r_{ij}$ is the normalized center of mass distance. This interaction adds chirality to the system, which is tuned by the parameter $\epsilon > 0\,k_BT$. The chiral potential is minimal for angles of $\pi/4$ between rods, leading to twists in the equilibrated membranes: Rods tilt and arrange themselves in a membrane-spanning vortex. These twists also form in absence of the chiral potential: They occur in right- and left-handed form in membranes of achiral rods due to an interplay between interfacial energy, elastic deformation energy, and entropic contributions. Yet a common sense of twist direction can be gradually induced using the chiral interaction.

This study employs Metropolis Monte Carlo (MC) simulations in the semigrand $N\mu_D VT$ ensemble and three-dimensional periodic boundary conditions. Each rod may translate or rotate, and the maximum displacement and rotation angle are adjusted to have acceptance rates of about 0.5 for each type of move. In addition to these single-particle moves, a "box move" is applied on average once per MC sweep. That is, the lengths of the sides of the simulation box are slightly changed while keeping the volume constant, and the rod centers of mass are rescaled accordingly; the y and z dimensions are kept equal to not deform the shape of the fibril cross section. The reason for adding the box move is that the height of the individual membranes depends on the total interaction (depleting plus chiral). Thus the fibril can only relax if the box's length in x direction, L_x, is not fixed but self-determined. A discussion about the influence of the initial box length and fixing the box length can be found in the Appendix (A 2). To relax and equilibrate the systems, we use several 10^5 MC sweeps, and for the main results, the averages were taken from 16 independent simulation runs and values recorded over 1–2 $\times$ 10^5 MC sweeps.

III. RESULTS

This paper mainly presents results for varying chiral strength ε, keeping the fibril dimensions and depletant concentration constant. From studies of isolated colloidal membranes, it is well known that the rodlike particles within do not all stand upright but twist towards the edge of the membrane [7,15,16]. The reason is the competition of elastic deformation energy, surface energy, and surface anchoring that scale differently with the membrane volume and surface. The surface energy describes the contribution due to the presence of the surface, while the surface anchoring contribution accounts for the orientation of rods with respect to the surface. The twisting also appears in the fibrils (stacks of membranes) and is the main topic of the current study. For a theoretical description of the fibrils in terms of free energy contributions, one would need to include the surface-surface interaction between membranes in addition to the terms used, for instance, in Ref. [7]. Here we do not estimate this from microscopic principles but discuss the results in terms of a comparison to the Ising model.

The direction of twist of the individual membranes is (in most situations) fixed during the initial equilibration. In the achiral case, $\varepsilon = 0\,k_BT$, there is a 50% chance to find left-handed membranes, but with increasing chiral strength, a higher percentage of membranes is left handed. The handedness parameter quantifies this fact:

$$R^{\ell r} = \frac{N^\ell - N^r}{N_M},$$

where $N^\ell(N^r)$ is the number of left-(right-)handed membranes. As can be seen in Fig. 2, for $\varepsilon \gtrsim 8\,k_BT$ all membranes are left-handed and the strongest effect of the chiral strength is found for $2 < \varepsilon/k_BT < 5$. Typically, the handedness is not changed once the twist is developed. Therefore, we resolve the measured quantities with respect to the number of left-handed membranes.

In addition to quantifying the fraction of left-handed membranes, it is interesting to study their distribution along the fibril. The two extreme cases are (i) all left-handed membranes are stacked together so that there are only two (or zero for $R^{\ell r} = \pm 1$) interfaces between left- and right-handed membranes and (ii) the number of left-right interfaces is maximized by separating the left-handed membranes. To

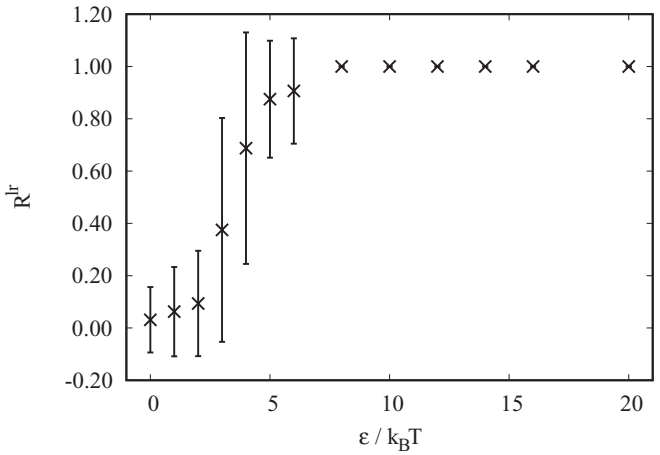

FIG. 2. Handedness parameter vs. chiral strength. Fibril dimensions are kept constant at $N_M = 4$ and $s_M = 6$ and the depletant density is $\rho_D = 2.31\,D^{-3}$. Error bars depict the standard deviation.

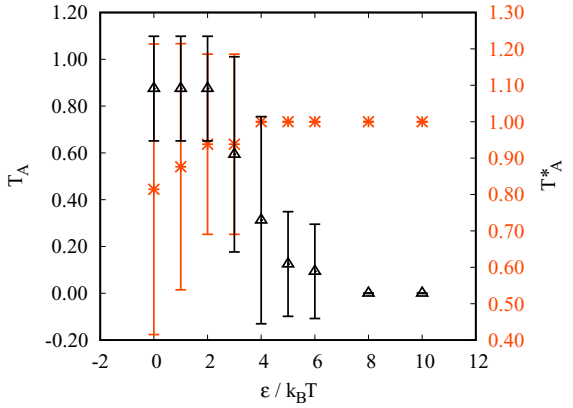

FIG. 3. (Normalized) twist alternation number vs. chiral strength. Fibril dimensions are kept constant at $N_M = 4$ and $s_M = 6$ and the depletant density is $\rho_D = 2.31\,D^{-3}$. Error bars depict the standard deviation. The normalized twist alternation number reaches its maximum already at $\varepsilon = 4\,k_BT$, while the plain twist alternation number still decreases and shows large error bars. The reason is that there are two, three, or four left-handed membranes, but in all cases, the number of twist alternations takes its maximum value (1, 0.5, and 0, respectively).

distinguish these cases, we introduce the twist alternation number:

$$T_A = \frac{N_C}{N_M},$$

where N_C is the number of left-right interfaces (C for *change* of twist direction). While this quantity is intuitive, it disregards that the fraction of left-handed membranes already restricts the number of possible twist alternations. In addition, the left-hand fraction is not (necessarily) constant for a fixed set of parameters. It is therefore expedient to include the minimum and maximum possible values, $T_{A,\min} = \frac{2\min(\min(N^\ell, N^\mathrm{r}), 1)}{N_M}$ and $T_{A,\max} = \frac{2\min(N^\ell, N^\mathrm{r})}{N_M}$, to get a normalized quantity:

$$T_A^* = \frac{T_A - T_{A,\min}}{T_{A,\max} - T_{A,\min}}$$

[Note that $T_{A,\min}$ and $T_{A,\max}$ are resolved with respect to N^ℓ, so that results for T_A^* are given as average of $T_A^*(N^\ell)$ over N^ℓ.] In the achiral case one could expect T_A to be 0.5, assuming that neither a change of twist direction nor its preservation is preferred. But this is not the case (not even close to), as shown in Fig. 3. Thus we conclude that there is a preference for changing the twist direction between consecutive membranes. This reminds us of the antiferromagnetic Ising model, where left- and right-handed membranes represent spin up and down. The respective Hamiltonian for the achiral case reads

$$H(\{s\}) = -J\sum_{i=1}^{N_M-1} s_i s_{i+1} - J s_{N_M} s_1,$$

with the coupling constant $J < 0$ and $s_i = \pm 1$. $\{s\}$ is a short notation for the state given by all the s_i, $i = 1, \ldots, N_M$. In this comparison, J quantifies the energy difference between neighboring membranes having the same handedness and neighboring membranes having an opposite handedness. The theoretical twist alternation number using this Ising description is

$$T_{A,\mathrm{Is}} = \langle N_M - \sum_{i=1}^{N_M-1} s_i s_{i+1} - s_{N_M} s_1\rangle/(2N_M)$$
$$= 1/2 + \langle H\rangle/(2JN_M),$$

where the brackets denote the canonical ensemble average. The average energy is found from the partition function, $\langle H\rangle = -\partial \ln Z/\partial\beta$, with $\beta = 1/k_BT$ and

$$Z = \sum_{\{s\}} \exp\left[-\beta H(\{s\})\right]$$
$$= [2\cosh(\beta J)]^{N_M} + [2\sinh(\beta J)]^{N_M}.$$

A similar relation can be derived for the normalized twist alternation number $T_{A,\mathrm{Is}}^*$. We map the measured values of the twist alternation number to the theoretical values from the Ising model and find $J = -0.73\,k_BT$ (using theoretical and simulation results for T_A) or $J = -0.37\,k_BT$ (using theoretical and simulation results for T_A^*). Surely, it is questionable whether $N_M = 4$ is large enough for such a comparison. Therefore we also study fibrils with $N_M = 12$, 20, and 30 and summarize the results in Table I. There is a systematic deviation of J with the number of stacked membranes, but

TABLE I. Summary of the mapping between simulation results and Ising model, cf. Eq. (2). $\tilde{\varepsilon}$ denotes the dimensionless chiral strength ε/k_BT.

N_M	$J(T_A)/k_BT$	$J(T_A^*)/k_BT$	$C(\tilde{\varepsilon})/k_BT$
4	−0.73	−0.37	$\tilde{\varepsilon}^{1.5}/4.1$
12	−0.35	−0.33	$\tilde{\varepsilon}^{1.4}/4.2$
20	−0.47	−0.41	$\tilde{\varepsilon}^{1.2}/2.5$
30	−0.54	−0.55	$\tilde{\varepsilon}^{1.2}/2.5$

the mapped values from T_A and T_A^* agree well for all but the shortest fibril, and all values agree at least in the order of magnitude.

Thus, the coupling constant quantifies by how much a left-right alternation is preferred over keeping the twist direction. To complete the picture, we can also find this value from umbrella sampling simulations, where an alternating sequence is biased to a nonalternating sequence. More precisely, we take a fibril of $N_M = 4$ stacked membranes with alternating twist direction and force one of the left-handed membranes to become right-handed. Details can be found in the Appendix (A 1). There is a barrier between the two states (the untwisted state of a membrane) that makes it unlikely that the twist direction is changed once the fibril is relaxed. The height of this barrier is found to be approximately $23\,k_BT$, and the coupling constant J is related to the free energy difference between the alternating and nonalternating state: $4J = \Delta F_{\text{an}}$ (the factor 4 results from having two changes from alternation to nonalternation when inverting one membrane and $2J$ energy difference per changeover). We find $\Delta F_{\text{an}} = -2.46 \pm 0.38 k_BT$ and are thus very close to the coupling constants found from the mapping of the twist alternation number.

The antiferromagnetic coupling must have an entropic origin. We did several tests to identify microscopic explanations for the behavior: We studied the distribution of rods' centers of mass along the fibril axis for alternating and nonalternating sequences and measured local free volumes of rods in the membrane, which was biased to have a particular twist via the umbrella sampling. However, the differences between alternating and nonalternating sequences were not clear enough to identify the microscopic origin of the antiferromagnetic coupling. We conclude that the microscopic differences are very subtle, and much more statistics would need to be collected to make a significant statement.

Adding chirality to the system drives the membranes to become left handed, as can be seen from Figs. 2 and 3. In terms of the Ising model, this resembles adding an external field that supports one spin state:

$$H(\{s\}) = -J \sum_{i=1}^{N_M-1} s_i s_{i+1} - J s_{N_M} s_1 + C \sum_{i=1}^{N_M} s_i, \qquad (2)$$

with $C > 0$ (< 0) for supporting spin down (up). The partition function in this case is given by

$$Z = \lambda_+^{N_M} + \lambda_-^{N_M},$$

$$\lambda_+ = e^{\beta J} \cosh \beta C + \sqrt{e^{2\beta J} \sinh^2(\beta C) + e^{-2\beta J}},$$

$$\lambda_- = e^{\beta J} \cosh \beta C - \sqrt{e^{2\beta J} \sinh^2(\beta C) + e^{-2\beta J}},$$

and the twist alternation number reads

$$T_{A,\text{Is}} = 1/2 + \langle H \rangle / (2JN_M) - C\langle M \rangle / (2JN_M),$$

where the "magnetization" is $\langle M \rangle = -\partial \ln Z / \partial C / \beta$. From the simulation results (T_A and T_A^*) for different chiral strengths ε we can now get the field strength C. We find that C does not linearly depend on ε, but with an exponent slightly larger than 1, see Table I. To give an impression of the theoretical behavior of the twist alternation number in the vicinity of the mapped parameters J and C, we plot the graphs of $T_{A,\text{Is}}$ in Fig. 4. The strongest effect is found for $C = 1\,k_BT$, where the twist alternation number drops from about 0.9 to about 0.2 in the given range of J. For stronger chiral interaction, i.e., larger C, $|J|$ would need to be much larger to significantly increase the twist alternation number. However, in the relevant range of J and C that match the simulation result, both parameters tune the behavior of left- and right-handed membranes.

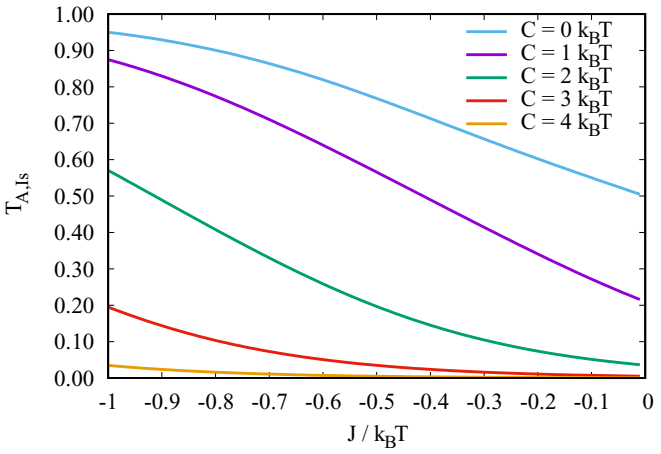

FIG. 4. Twist alternation number for the antiferromagnetic Ising model vs. coupling constant for different field strengths.

With increasing chiral strength (or similarly decreasing reduced temperature), the fibril contracts, as shown in Fig. 5. The relative reduction of the length is naturally rather low, but it is systematic and may add up to a relevant amount for many stacks. We believe that this contraction is one effect that may be utilized in functional materials. Left-handed membranes are shorter than right-handed ones, as is seen by the difference in the length for different compositions at the same chiral strength. The reason is that the system reduces the unfavored right-handed twist by making right-handed membranes twist less (and thus appear thicker). This effect can also be seen

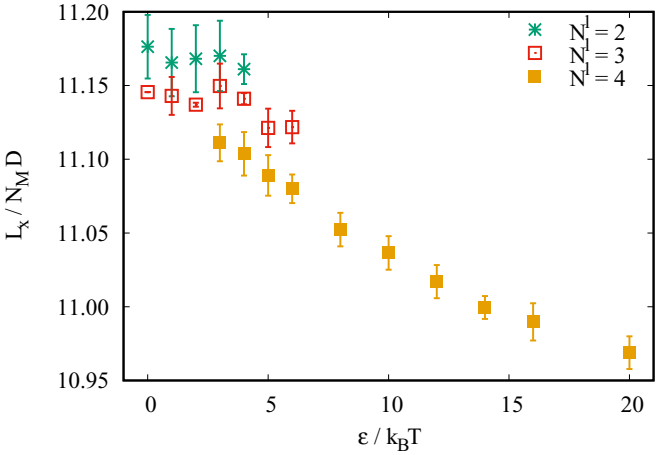

FIG. 5. Fibril length divided by number of stacked membranes vs. chiral strength. Fibril dimensions are kept constant at $N_M = 4$ and $s_M = 6$ and the depletant density is $\rho_D = 2.31\,D^{-3}$. The different symbols (and colors) denote different numbers of left-handed membranes, as indicated. Error bars depict the standard error of the mean.

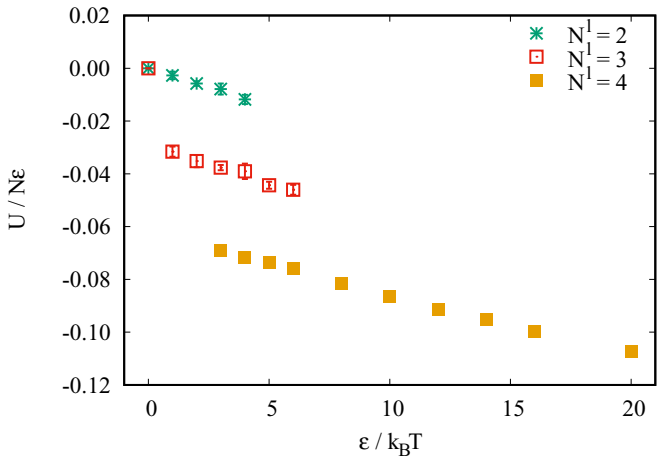

FIG. 6. Reduced potential energy of fibrils vs. chiral strength. Fibril dimensions are kept constant at $N_M = 4$ and $s_M = 6$ and the depletant density is $\rho_D = 2.31\,D^{-3}$. The different symbols (and colors) denote different numbers of left-handed membranes, as indicated. Error bars depict the standard error of the mean.

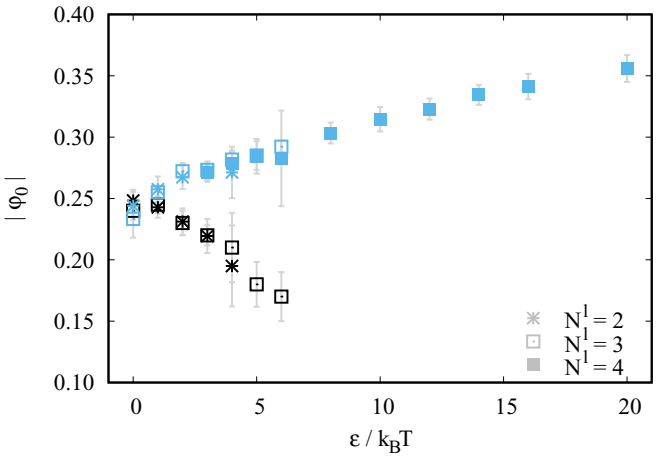

FIG. 7. Edge twist angle vs. chiral strength. Fibril dimensions are kept constant at $N_M = 4$ and $s_M = 6$ and the depletant density is $\rho_D = 2.31\,D^{-3}$. The different symbols denote different numbers of left-handed membranes, as indicated, and the color denotes the handedness [black: right, blue (gray): left]. Error bars depict the standard error of the mean.

in the potential energy, Fig. 6: The 50:50 mixture of left- and right-handed membranes does not have vanishing energy. Due to the symmetry of the interaction potential, given by Eq. (1), a mirror-imaged membrane has the same absolute value of the total energy as the original, but the energy has the opposite sign. That is, the left-handed and right-handed membranes are not simple inversions of each other, which is in accord with the difference in length discussed above. This also presents a caveat for the comparison to the Ising model: The energy difference between a left- and a right-handed membrane due to the "field" C is given by $2C$ in this model. In the actual system it is not that simple because of the feedback between the fraction of left-handed membranes, degree of twist, and chiral strength. For a fixed fibril composition, the reduced potential energy seems to decrease linearly.

To quantify the twist that all membranes show (even for $\varepsilon = 0\,k_BT$), we fit the azimuthally averaged twist angle profile to a simple form:

$$\varphi(r) = \varphi_0\left(\frac{r}{R}\right)^{\alpha},$$

so that φ_0 is the twist angle at the surface, which is on average at a distance R from the axis, and α determines the slope of the profile at the surface. For the systems in this study, we find $\alpha \approx 1$. The results in Fig. 7 show the expected behavior, i.e., with increasing chiral strength, the left-handed membranes twist more strongly, and the right-handed ones (if present) twist less.

Not only the chiral strength affects the results, but also the concentration of depleting spheres, which was kept constant at $\rho_D = 2.31\,D^{-3}$ so far. There is a lower bound on ρ_D, below which fibrils are not stable anymore and fall apart. Above that, fibrils twist less with increasing ρ_D, Fig. 8. The reason for this is the increase of the packing density towards hexagonal close packing, which is incommensurate with any twist and thus reduces φ_0. Remarkably, even at very high depletant density, some twist prevails, which we attribute to the enhancement of translational entropy due to rods moving along their tilted axes. However, the system shows a hexagonal order, which is measured with the hexagonal order parameter:

$$\Psi = \left| \frac{1}{N_r} \sum_{j=1}^{N_r} \frac{1}{b_j} \sum_{n \in nn_j} e^{i6\theta(n,j)} \right|,$$

where N_r is the total number of rods in the fibril, b_j is the number of nearest neighbors of rod j (6 in the center and <6 at the edge), nn_j the set of nearest neighbors of rod j and $\theta(n, j)$ the angle between a fixed axis and the connecting line of rods n and j, and can be seen in Fig. 9. It decreases rapidly below $\rho_D = 2/D^3$, where the fibril first becomes liquidlike, i.e., the positional order within the membranes reduces to

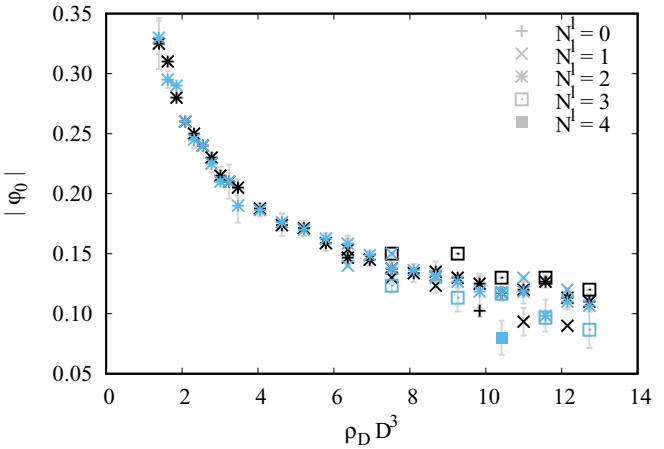

FIG. 8. Edge twist angle vs. depletant concentration for achiral rods. Fibril dimensions are kept constant at $N_M = 4$ and $s_M = 6$. The different symbols denote different numbers of left-handed membranes, as indicated, and the color denotes the handedness [black: right; blue (gray): left]. Error bars depict the standard error of the mean.

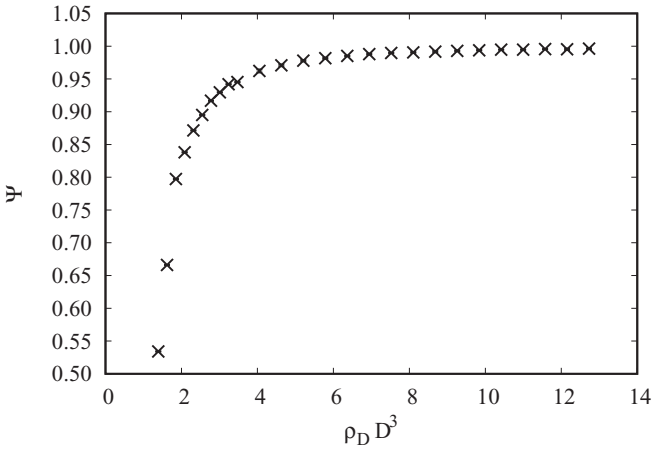

FIG. 9. Hexagonal order parameter vs. depletant concentration for achiral rods. Fibril dimensions are kept constant at $N_M = 4$ and $s_M = 6$. Error bars are absent for low ρ_D and depict the (very small) standard error of the mean from several simulations at high ρ_D.

short-range order while the membranes still stay stacked along the fibril axis. For even lower ρ_D the fibril starts to fall apart and loses any ordering. On the other hand, the hexagonal order parameter gets very close to one for large ρ_D, even though the membranes are still twisted.

We note that for $\rho_D > 4/D^3$ the fibrils contract along their long axis to an extent that the average length per membrane is less than the rod length. This means that the assumption of stacked, upright-standing rods in the membranes' twist centers has to be dropped. These centers might be shifted from the central axis, or all rods within a membrane are tilted. Either way, the system's cylindrical symmetry must be broken. We do not elaborate on this here but use it to motivate the strong fluctuations of φ_0 at high depletant concentration.

A comparison to and a brief discussion of the behavior of isolated membranes is given in the Appendix (A 3).

IV. CONCLUSION

We have studied the influence of the strength of a chiral interaction between rodlike particles on the properties of thin smectic fibrils by employing Monte Carlo simulations. The fibrils are composed of hexagonally shaped colloidal membranes that are stacked face to face. An attractive depletion interaction due to the presence of Asakura-Oosawa spheres stabilizes the whole assembly.

Like in isolated colloidal membranes, the rods within the stacked membranes twist towards the fibril surface, even for vanishing chiral interaction. This effect is based on the interplay between surface energy, elastic deformation energy, and entropic effects. In the achiral case, the number of membranes with left- and right-handed twist is balanced, and an alternation of twist direction along the fibril is preferred. We compared this result with the antiferromagnetic Ising model and could determine coupling constants that agree with umbrella sampling results of the free energy difference between alternating and nonalternating twist directions. An increasing chiral strength gradually increases the fraction of left-handed membranes to 1 and thus takes the role of an external field in the Ising model comparison.

The chiral interaction tunes not only the twist direction but also the length of the fibril: The fibril contracts on increasing the chiral strength (or similarly decreasing the temperature). We believe that this effect could find application in stimuli-responsive self-assembled materials. However, we are not aware that it has been seen in experiments so far, presumably due to small absolute differences and low reduced chiral strength. Also, the sequence of left- and right-handed membranes may be used to encode information: Because of the high barrier between alternating and nonalternating sequences, the system will not change the overall sequence for weak, reduced chiral strengths, but will do so on increasing this strength.

Besides, all effects depend on the depletant concentration, giving another possibility also experimentally to tune the behavior. For the paper at hand, we did the detailed study only for one depletant concentration because the results are expected to be of similar quality for a range of concentrations.

ACKNOWLEDGMENTS

We thank Tanja Schilling and Eric Grelet for helpful discussions and inspiring ideas regarding this project. Support by the state of Baden-Württemberg through bwHPC and the German Research Foundation (DFG) through Grant No. INST 39/963-1 FUGG (bwForCluster NEMO) is acknowledged.

APPENDIX

1. Umbrella sampling of twist inversion

In order to understand whether the coupling of the handedness of neighboring membranes depends on the equilibration protocol, we did several tests: letting membranes relax consecutively one after the other, having only two membranes relax while the others are held fixed, and changing the simulation box length. The results were not unambiguous, so we performed umbrella sampling simulations to determine the free energy difference between alternating and nonalternating twist direction of consecutive membranes along the fibril. For a proper review on the umbrella sampling technique, we refer to Ref. [20]. The fibril consists of four membranes, initially with alternating twist directions, and one of them is forced to change its twist direction. Biasing coordinates are chosen to measure the strength of the twist, including its direction, and the slope of the twist angle profile at the membrane surface. The latter is necessary to ensure that the reversed membrane also shows an almost linear twist angle profile, as does the initial, relaxed one. The strength of twist is measured as the average squared x component of the unit orientation vectors of all N_m rods in the membrane, $m_x^2 = \langle \sum_{i=1}^{N_m} m_{i,x}^2 / N_m \rangle$, where the brackets denote an average over a few Monte Carlo sweeps. A left- and a right-handed membrane are distinguished by the parameter s being -1 or $+1$, respectively. The combined reaction coordinate reads $m_s = s m_x^2 + 1 - s$, and is 1 for an untwisted membrane, >1 for a left-handed one and <1 for a right-handed one. To get useful statistics over the whole range of m_s, we subdivide the range into several overlapping windows. In each of them, the system is biased to have values of

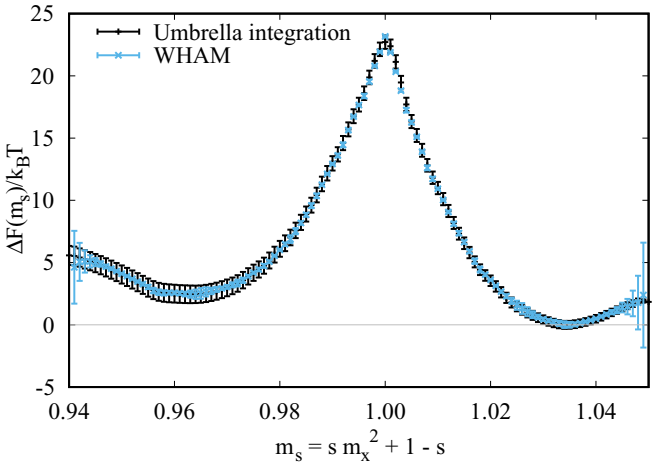

FIG. 10. Free energy barrier between a fibril with only alternating twist directions (rlrl, $m_s \approx 1.035$) and a fibril with less alternations (rrrl, $m_s \approx 0.964$). Fibril dimensions are $N_M = 4$ and $s_M = 6$ and the depletant density is $\rho_D = 2.31\,D^{-3}$. The s in the definition of m_s is $+1$ if the second membrane is right handed and -1 if it is left handed. Umbrella sampling results are analyzed by a weighted histogram analysis method (WHAM) and the umbrella integration technique.

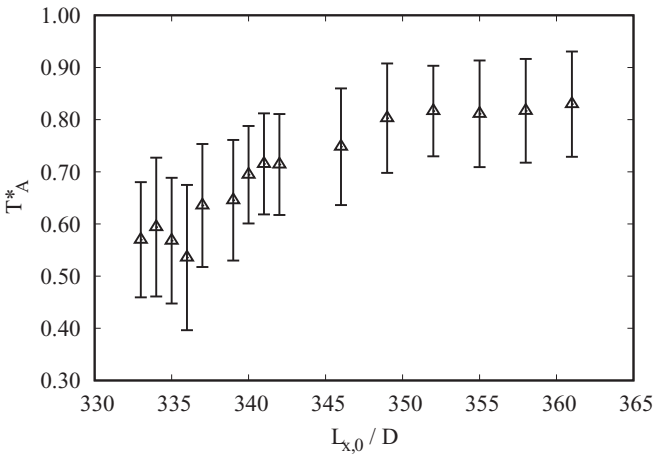

FIG. 11. Normalized twist alternation number vs. initial box length for the achiral case ($\varepsilon = 0\,k_BT$). Fibril dimensions are $N_M = 30$ and $s_M = 6$ and the depletant density is $\rho_D = 2.31\,D^{-3}$.

m_s in that window, and it is moderately biased to have a linear twist angle profile. The biasing potential is harmonic, with its minimum in the center of the window. Its strength is chosen such that the window center is sampled sufficiently and overlap to neighboring windows is assured, which gets more intricate around $m_s = 1$, where more windows and stronger biasing are needed.

The umbrella sampling results in all the windows need to be combined to get the free energy differences over the whole range of m_s. There are several techniques to do that, but the most commonly used ones are weighted histogram analysis (WHAM) and umbrella integration, cf. Ref. [20] and references therein. The main difference is that in WHAM, the free energy data from the different windows are shifted and combined to minimize the statistical error of the global distribution of reaction coordinates. In contrast, in umbrella integration, the mean forces are averaged over the windows, and the free energy is found by integration. Here we show the resulting barrier for both methods in Fig. 10. The agreement is excellent, but in the vicinity of $m_s = 1$, we needed many simulation data to get reliable values. Error bars are estimated based on the discussions in Refs. [21,22].

2. Influence of initial box length

As described in the simulations section, the length of the simulation box is allowed to fluctuate to reduce stress imposed by the periodic boundaries (self-determined box length). However, we found that the results depend on the initial box length, especially for long fibrils. As an example, Fig. 11 shows the normalized twist alternation number vs. the initial length of the box. The alternation of twist direction is suppressed for small initial box lengths. This is somewhat unexpected because one would assume that close-by membranes interact more strongly and follow the (slightly) preferred twist alternation. We explain the reduction of T_A^* by the fact that for small $L_{x,0}$ the box length increases at the beginning of the simulation, while for large $L_{x,0}$ it decreases from the start. That is, for the former, it is more critical for the system to stretch than to follow the preferred twist direction, and for the latter shrinking the length and twist alternation accompany each other. This is also supported by the fact that the surface twist angle decreases with increasing fibril length to prevent the creation of additional surfaces between membranes, as illustrated by a sketch in Fig. 12. One could ask why at all the rods twist at the fibril surface at the risk of creating more surface. We think that this is due to an increase in translational entropy: tilted rods can move a larger distance along their axis compared to untilted rods for the same membrane distance. We tested the length-twist relation by fixing the fibril length (no relaxation) to different values in a range around the average equilibrium length from the self-determined simulations. There is a clear dependence: φ_0 monotonically decreases from about 0.25 for the smallest length (close to maximal packing)

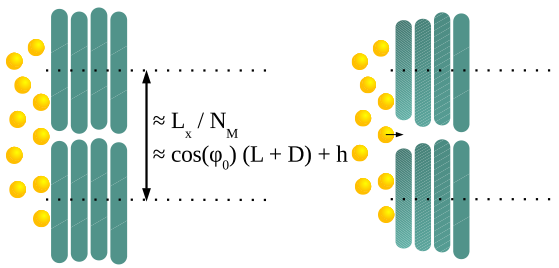

FIG. 12. Sketch of a fibril of length L_x showing the hypothetical gap between membranes due to a high twist angle φ_0. The average distance between membrane center planes is L_x/N_M. At the surface, a gap of height h between the membranes appears that depends on the average membrane distance and on the surface twist angle. To avoid the formation of additional surfaces between membranes, the gap needs to be smaller than the depletant diameter. This in turn constrains φ_0 to smaller values for larger fibril lengths. Left: $\varphi_0 = 0$, right: $\varphi_0 > 0$.

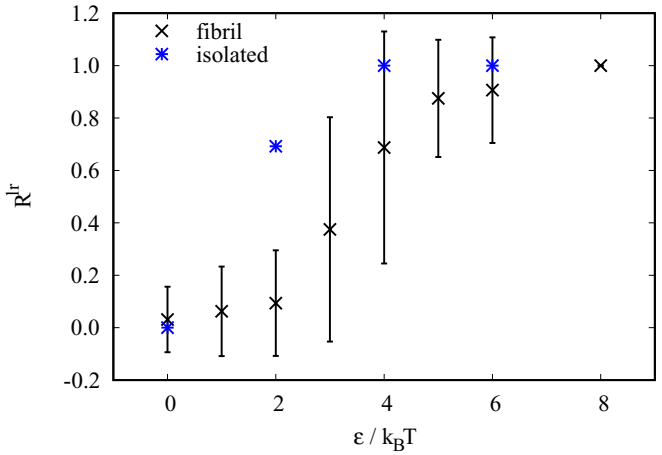

FIG. 13. Comparison of the handedness parameter for membranes stacked to a fibril (black crosses) and isolated membranes with the same size (blue stars) $s_M = 6$ at a depletant density of $\rho_D = 2.31\,D^{-3}$.

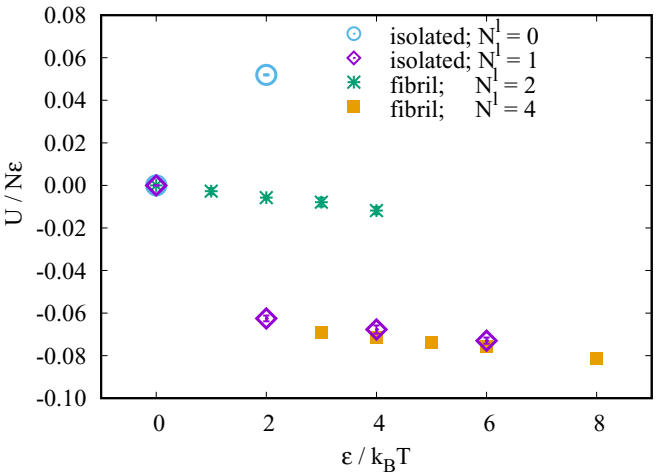

FIG. 14. Comparison of the reduced potential energy for membranes stacked to a fibril and isolated membranes with the same size $s_M = 6$ at a depletant density of $\rho_D = 2.31\,D^{-3}$. The different symbols (and colors) denote different numbers of left-handed membranes, as indicated.

to about 0.18 for a length close to the rupture length, where the membranes separate from each other and destroy the fibril.

The simulations of the results presented in the main text were started with an initial length per membrane of $L_{x,0}/N_M = 11.625\,D$, where we expect (from Fig. 11) the results to be independent on further increase of the initial length.

3. Comparison to isolated membranes

Isolated colloidal membranes have already been studied [7,15,16]. However, for a direct comparison of the behavior of stacked and isolated membranes, it is advantageous to simulate isolated membranes with the same parameters. The simulations are identical to those of the stacked membranes; only the periodic boundaries do not have an effect anymore because the isolated membranes are centered in the simulation box, which is much larger than the membrane. The initial setup is the same, too, i.e., rods are aligned in the same direction and placed on a hexagonal lattice. The results shown are found from up to 16 independent runs.

First, we compare the handedness parameter in Fig. 13. For the isolated membranes, this is defined as the difference between the number of left- and right-handed membranes divided by the number of independent runs. In the isolated case, a chiral strength of $\varepsilon = 4\,k_BT$ is sufficient to have 100% left-handed membranes, while in the stacked case $\varepsilon = 8\,k_BT$ is needed. Already for $\varepsilon = 2\,k_BT$, the isolated membranes show a much larger fraction of left-handed membranes compared to the stacked ones. This is another proof of the antiferromagnetic coupling of neighboring membranes.

Similarly, we compare the reduced potential energy in Fig. 14. There are two things to note: As for stacked membranes and as expected, the absolute value of the energy of isolated membranes is larger for a left-handed one compared to a right-handed one (as seen for $\varepsilon = 2\,k_BT$). Besides, the absolute energy value is slightly smaller in the isolated membranes compared to the stacked ones. This means that the free surface in the isolated case causes the rods to take an energetically less preferred configuration in order to reduce the surface contribution to the free energy.

The edge twist angle φ_0 slightly depends on the membrane situation (isolated or stacked) and is a bit larger in the isolated case, as can be seen in Fig. 15. A more apparent difference is found for the area number density, $\rho_0 = N_r/(\pi R^2)$, where N_r is the number of rods per membrane and R is an effective radius found from assuming azimuthal symmetry. As shown in Fig. 16, the isolated membranes appear to be denser with an ε-dependent density, while the stacked membranes have a constant (lower) density. In addition to comparing the isolated and stacked membranes, we also briefly discuss the influence of membrane size and depletant density on the isolated membranes. A more detailed study about isolated membranes will be published elsewhere [16]. Figure 17 shows the membrane area density for numbers of rods per membrane $N = 91$, 397, and 919, and for three different depletant densities as a

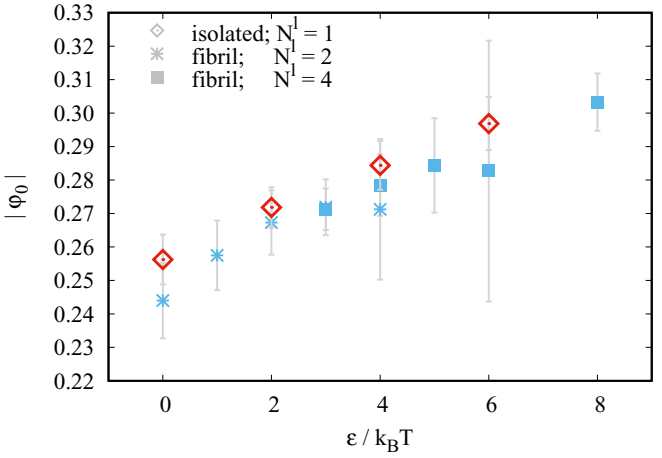

FIG. 15. Comparison of the edge twist angle for membranes stacked to a fibril and isolated membranes with the same size $s_M = 6$ at a depletant density of $\rho_D = 2.31\,D^{-3}$. We only show results for left-handed membranes and $N^\ell = 2$ and 4.

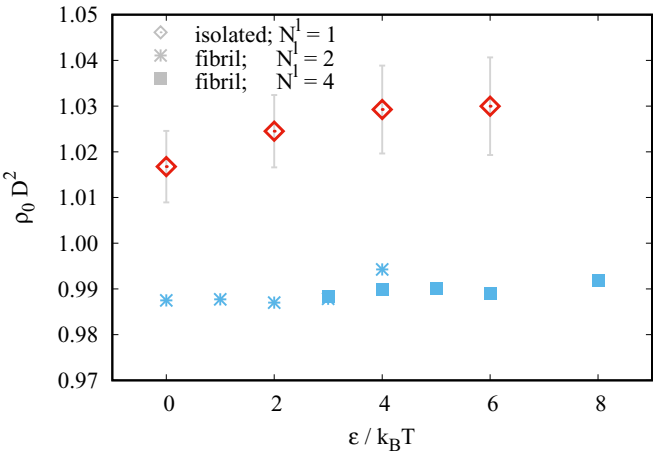

FIG. 16. Comparison of the area number density for membranes stacked to a fibril and isolated membranes with the same size $s_M = 6$ at a depletant density of $\rho_D = 2.31\,D^{-3}$. We only show results for left-handed membranes and $N^\ell = 2$ and 4.

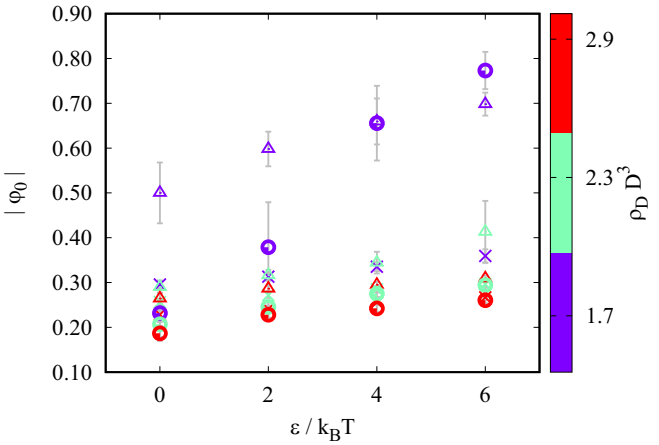

FIG. 18. Edge twist angle for isolated membranes vs. chiral strength for different depletant densities (color) and different numbers of rods (symbols: cross: $N = 91$; triangle: $N = 397$; circle: $N = 919$). We only show results for left-handed membranes.

function of the chiral strength ε. As expected, for fixed N and ε, the density increases with increasing depletant density. The membrane density is higher for the smallest N compared to the two larger numbers, where the densities almost agree. Most interesting is the behavior with ε: The density increases with ε for the smallest system at the medium and high depletant concentration (red and green crosses); it is almost constant for the larger systems at the highest ρ_D (red triangles and circles); it slightly decreases for the larger systems at the medium ρ_D (green triangles and circles) and the small system at the lowest ρ_D (blue crosses); and it clearly decreases for the larger systems at the lowest depletant density (blue triangles and circles).

An explanation for the latter can be found by looking at the edge twist angle, Fig. 18. For the two larger membranes at the lowest depletant density, the edge twist angle strongly increases with the chiral strength ε. This is only possible because the membranes lose the hexagonal ordering and become more fluidlike. That means there is an order-disorder transition below $\rho_D = 2.3\,D^{-3}$, which is, however, not seen in the smallest system. The stronger twist in the fluidlike membranes decreases the (average) membrane density because tilted rods take more space when projected on the membrane's central plane. The slight increase of ρ_0 with ε for some systems is due to the attractiveness of the chiral interaction potential.

Not only the edge twist angle but also the shape of the twist angle profile changes with membrane size and depletant density. This is quantified by the curvature parameter α, which is a fitting parameter for the twist angle profile $\varphi(r) = \varphi_0(r/R)^\alpha$, where R again is the approximated radius. The result for a fixed chiral strength is shown in Fig. 19. For the smallest systems, α is close to 1 independent of ρ_D, i.e., the profile is close to linear. For the ordered membranes ($\rho_D \geqslant 2.3\,D^{-3}$), α increases slightly with the number of rods, and for the fluidlike membranes, the curvature is clearly stronger.

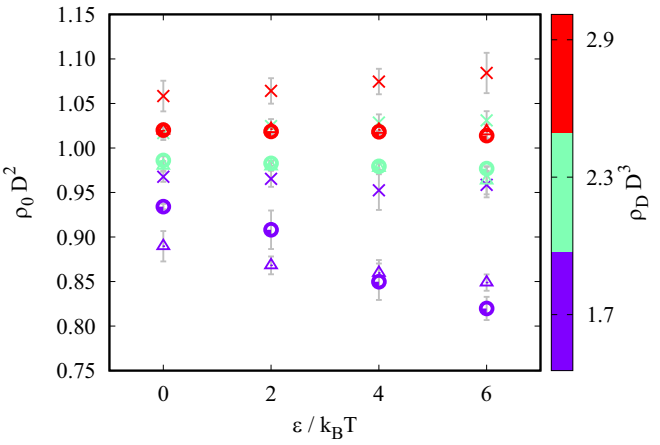

FIG. 17. Area number density for isolated membranes vs. chiral strength for different depletant densities (color) and different numbers of rods (symbols: cross: $N = 91$; triangle: $N = 397$; circle: $N = 919$). We only show results for left-handed membranes.

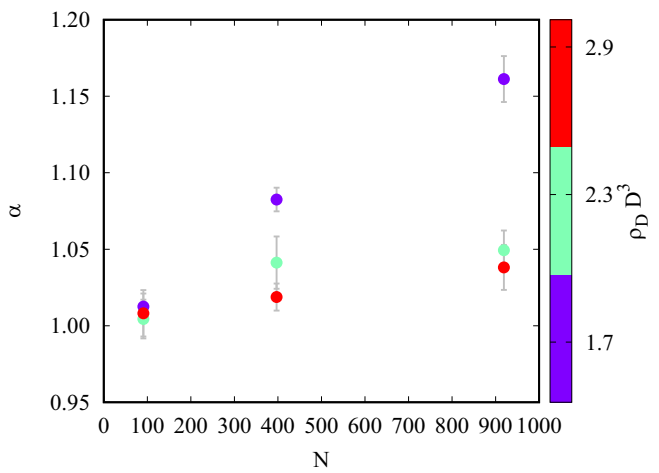

FIG. 19. Curvature parameter for isolated membranes vs. number of rods for different depletant densities (color) and a chiral strength of $\varepsilon = 6\,k_BT$.

It is expected that in the fibril system (i.e., stack of membranes), the described effects are much weaker due to the membranes' face-face interaction. However, it would be interesting to study the stability of fibrils composed of fluidlike membranes in the future.

[1] Z. Dogic and S. Fraden, Ordered phases of filamentous viruses, Curr. Opin. Colloid Interface Sci. **11**, 47 (2006).

[2] Z. Dogic, Filamentous phages as a model system in soft matter physics, Front. Microbiol. **7**, 1013 (2016).

[3] B. Sung, A. de la Cotte, and E. Grelet, Chirality- controlled crystallization via screw dislocations, Nat. Commun. **9**, 1405 (2018).

[4] M. Adams and S. Fraden, Phase behavior of mixtures of rods (tobacco mosaic virus) and spheres (polyethylene oxide, bovine serum albumin), Biophys. J. **74**, 669 (1998).

[5] E. Barry and Z. Dogic, Entropy driven self-assembly of nonamphiphilic colloidal membranes, Proc. Natl. Acad. Sci. USA **107**, 10348 (2010).

[6] Y. Yang, E. G. Barry, Z. Dogic, and M. F. Hagan, Self-assembly of 2d membranes from mixtures of hard rods and depleting polymers, Soft Matter **8**, 707 (2011).

[7] L. Kang, T. Gibaud, Z. Dogic, and T. C. Lubensky, Entropic forces stabilize diverse emergent structures in colloidal membranes, Soft Matter **12**, 386 (2016).

[8] T. Gibaud, Filamentous phages as building blocks for reconfigurable and hierarchical self-assembly, J. Phys.: Condens. Matter **29**, 493003 (2017).

[9] B. Sung, H. Wensink, and E. Grelet, Depletion-driven morphological transitions in hexagonal crystallites of virus rods, Soft Matter **15**, 9520 (2019).

[10] Persistence of Vision Pty. Ltd., (2004) Persistence of Vision Raytracer (Version 3.6), http://www.povray.org/download/.

[11] E. Grelet and S. Fraden, What is the Origin of Chirality in the Cholesteric Phase of Virus Suspensions? Phys. Rev. Lett. **90**, 198302 (2003).

[12] E. Barry, D. Beller, and Z. Dogic, A model liquid crystalline system based on rodlike viruses with variable chirality and persistence length, Soft Matter **5**, 2563 (2009).

[13] D. Frenkel and T. Schilling, Smectic filaments in colloidal suspensions of rods, Phys. Rev. E **66**, 041606 (2002).

[14] S. V. Savenko and M. Dijkstra, Phase behavior of a suspension of colloidal hard rods and nonadsorbing polymer, J. Chem. Phys. **124**, 234902 (2006).

[15] H. H. Wensink and L. Morales Anda, Elastic moduli of a smectic membrane: A rod-level scaling analysis, J. Phys.: Condens. Matter **30**, 075101 (2018).

[16] A. Kuhnhold, N. Göth, and N. Helmer, Colloidal membranes of chiral rodlike particles (unpublished) (2021).

[17] J. Glaser, A. S. Karas, and S. C. Glotzer, A parallel algorithm for implicit depletant simulations, J. Chem. Phys. **143**, 184110 (2015).

[18] W. J. A. Goossens, A molecular theory of the cholesteric phase and of the twisting power of optically active molecules in a nematic liquid crystal, Mol. Cryst. Liq. Cryst. **12**, 237 (1971).

[19] A. Varga and G. Jackson, Simulation of the macroscopic pitch of a chiral nematic phase of a model chiral mesogen, Chem. Phys. Lett. **377**, 6 (2003).

[20] J. Kästner, Umbrella sampling, WIREs Comput. Mol. Sci. **1**, 932 (2011).

[21] J. Kästner and W. Thiel, Analysis of the statistical error in umbrella sampling simulations by umbrella integration, J. Chem. Phys. **124**, 234106 (2006).

[22] J. Kästner, Umbrella integration in two or more reaction coordinates, J. Chem. Phys. **131**, 034109 (2009).